# Equivalent Circuit Model of High Power LEDs for VLC Systems

Xicong Li[1], Zabih Ghassemlooy[1], Stanislav Zvanovec[2], Min Zhang[3], Andrew Burton[1]
[1]*Optical Communications Research Group, Northumbria University*, Newcastle upon Tyne, UK
[2]*Czech Technical University in Prague*, Prague, Czech Republic
[3]*Beijing University of Posts and Telecommunications*, Beijing, China
[1]xicong.li, z.ghassemlooy, andrew2.burton@northubria.ac.uk, [2]xzvanove@fel.cvut.cz, [3]mzhang@bupt.edu.cn

***Abstract*—The equivalent circuit model for two commercial high power LEDs for illuminance is proposed and extensive measurements have been carried out to verify the accuracy of the model. In addition, the frequency response of two LEDs in the optical domain can be estimated using the transfer function of electrical equivalent circuit. It is shown that, the electrical parasitics in the chip and packaging introduce significant attenuation beyond a resonance frequcency. Care should be taken when designing high-speed driver and/or equalization circuits for VLC systems.**

***Index Terms*—LED, equivalent circuit, impedance, impedance matching, driver circuit, bandwidth, carrier lifetime, VLC**

## I. Introduction

Light emitting diodes (LEDs) have been intensively investigated since Burrus [1] fabricated the first LED for optical fiber communication systems. LEDs with high luminous and energy efficiencies compared to traditional light sources of incandescence and fluorescence, color rendering, reduced size and lower cost are currently being adopted in a wide range of applications. In addition, LEDs *(i)* light output can be changed or dimmed by simply adjusting the drive current up to the rated maximum level; and *(ii)* offer longer life span. LEDs can have vastly different characteristics with regard to, for example, the frequency response (i.e., switching speed), luminous, colour rendering and efficiency. As for the LED's frequency response, it is well known that its frequency response follows the first order system [2]–[5], whereby its modulation bandwidth is mainly limited by the effective carrier lifetime which is typically 2-5 ns for InGaAsP LEDs [6] with a corresponding bandwidth up to hundreds of MHz.

In recent years, we have seen a growing research interest in the emerging wireless technology of visible light communications (VLC), which uses both solid state and organic LEDs at the transmitter [7], [8]. VLC offers illumination, data communication, indoor localization and sensing. However, LEDs used for illuminance tend to have large areas (i.e., high capacitance) and operate at high drive current, thus imposing a modulation bandwidth limit and driving complexity. On the other hand, LEDs for data communications should be small in size with low capacitance and much reduced parasitic elements. Research on white LEDs for VLC systems has mainly focused on algorithms, system implementation and performance evaluation. However, not much has been reported on the frequency response of LED devices within the context of VLC systems.

The equivalent circuit model of the LED is of practical importance for designing efficient driver and/or modulation circuits as well as equalizers to extend modulation bandwidth. The one port reflection measurement is an efficient approach based on the S11 parameter to characterize the impedance and carrier lifetime of lasers and LEDs [9]–[13]. In [14], [15], this method was adopted to characterize the equivalent circuit of AlGaN based multiple quantum well (MQW) deep ultraviolet (UV) and double heterojunction (DH) LEDs. However, there is limited information in the literature on the equivalent circuit characterization of high-power LEDs used in VLC systems. Note that, here generally high-power LEDs refer to those with a single chip size not less than 1 $mm^2$ with a drive current of at least 350 mA [16]–[18]. In this paper we investigate the effects of parasitic elements on modulation bandwidth in high-power LEDs within the context of VLC.

The rest of the paper is organized as following. The equivalent circuit model is given in Section II and measured results are shown in Section III as well as fitted element values.

## II. Small signal model

### A. Theory

A practical LED chip can be modelled as a parallel $RC$ circuit [5, 6, 20, 21]. The resistance can be obtained from the differential resistance $r_d$ of LED's intrinsic *p-n* junction, while the capacitance consists of the space-charge capacitance $C_{sc}$, which results in the delay of carrier injection to the *p-n* junction, and the diffusion capacitance $C_d$. The ultimate limit of LED modulation bandwidth is determined by the carrier recombination lifetime $\tau = r_d C_d$ . Due to the parasitic $C_{sc}$, the frequency response of the LED is given by:

$$H(w) = \frac{1}{1 + j\omega\tau_{\text{eff}}} \tag{1}$$

where $\tau_{\text{eff}} = r_d(C_d + C_{sc})$ is the effective carrier lifetime, $\omega$ is the angular frequency, and $j = \sqrt{-1}$.

In addition, real LED chips have a series resistance due to current crowding under electrodes, ohmic contacts and bonding wires from the die [19]. Large size LEDs, especially high-power LEDs used in VLC systems, tend to have a large $C_{sc}$ between the layers and a parasitic capacitance $C_e$ between

electrodes as shown in Fig. 1 (note, $C_e$ depends on the LED chip design).

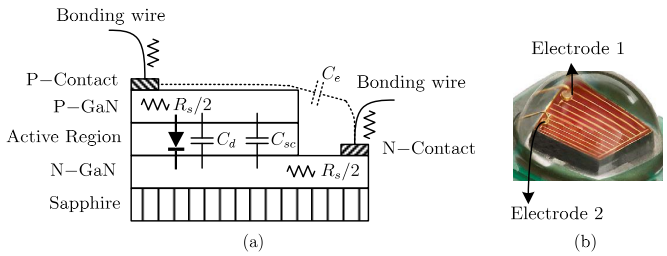


Fig. 1. A conventional LED: (a) Chip structure, and (b) A Red LED (from Cree XPE®)

### B. Packaging

For high-power LEDs with large areas, packaging is important to ensure good heat dissipation and therefore longer lifetime. Commercial high power LED chips are available in mainly three packages of conventional package, flip-chip package and vertical package [16]. A red and a white LED are considered in this paper. The red LED (Cree XPERED-L1-0000-00501) with the conventional chip package and rectangular electrodes is shown in Fig. 1(b), while the white LED (Lumileds Luxeon Rebel LXML-PWC2) has a flip-chip package with the phosphor coated on the GaN blue LED chip. External packages for the chips are availble in a wide variety of ways. Both devices considered here are based on chip-on-ceramic board packaging in order to minimize the physical size [17].

An electrostatic discharge (ESD) protection diode (e.g., Zener diodes) is another important component in LED packaging to protect the chip from damage. It comes in different combination with different parasitic [19]. The ESD parasitic capacitance is included within the total bonding capacitance $C_b$ together with the electrode capacitance $C_e$. Note that here the ESD is modelled as a single capacitance for simplicity and its accurate model cannot be obtained due to its integration in the package. Common ESD diodes will have a capacitance of 500 pF to 10 nF with a zero bias, which can contribute to the distortion of high-speed signals beyond the operating frequency of 500 MHz.

### C. Equivalent Circuit Model

The equivalent circuit for high power LEDs is shown in Fig. 2. The intrinsic LED model is composed of the differential resistance $r_d$ and the junction capacitance $C_j$, which is the sum of the space-charge capacitance $C_{sc}$ and the diffusion capacitance $C_d$ . The parasitic consists of the series resistance $R_s$ inside the LED chip, the series bonding resistance $R_b$, the series bonding inductance $L_b$ and the parallel bonding capacitance $C_b$ . Note that $R_g$ is the impedance of the source (50 Ω for the vector network analyzer, VNA).

The impedance of an LED is given by:

$$Z_{\text{LED}} = R_b + j\omega L_b + \frac{1}{j\omega C_b} // \left( R_s + \frac{1}{j\omega C_j} // r_d \right) \quad (2)$$

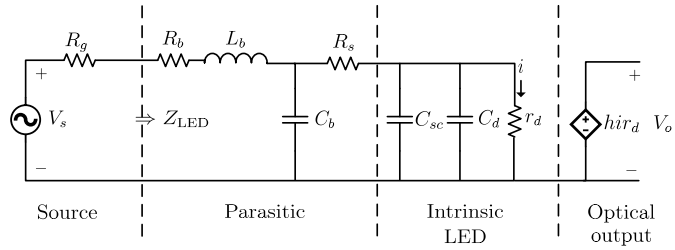


Fig. 2. The equivalent circuit model for the AC small signal.

where $C_j = C_{sc} + C_d$ is the junction capacitance.

### D. Modulation Characteristics

The optical output can be obtained from (2) based on the fact that optical power is proportional to the current $i$ through the differential resistance, which is representative of effective modulated current through the active region. The output voltage $V_o = hir_d$ in Fig. 2 can be considered as the small-signal light output intensity of the LED [3], [10], where $h$ is the gain coefficient. Therefore, the frequency response of the LED (including packaging) can be modelled using the voltage transfer function as given by:

$$\begin{aligned} H_{\text{LED}}(s) = \frac{V_o(s)}{V_s(s)} &= h\frac{r_d}{Z_{\text{LED}} + R_g} \\ &= 1/\Bigg( s^3 R_s L_b C_j C_b \\ &\quad + s^2\left[R_b + R_g + R_s C_j C_b + L_b\left(C_b\frac{R_s + r_d}{r_d} + C_j\right)\right] \\ &\quad + s\left[R_b + R_g + \left(C_b\frac{R_s + r_d}{r_d} + C_j\right) + \frac{L_b}{r_d} + R_s C_j\right] \\ &\quad + \frac{r_d + R_b + R_g + R_s}{r_d}\Bigg) \end{aligned} \quad (3)$$

where $s = j\omega$ is the complex variable.

To verify the validity of this method, the S21 parameter was measured and compared with estimated response as presented in the section III. It is interesting to notice that the LED's response follows the first-order *RC* system at low frequencies, and attenuates significantly as a three-order system above the resonance peak caused by parasitic elements. From the standpoint of driver or equalizer design, more gain should be provided to compensate for the parasitic introduced attenuation.

## III. Measurement Setup and Results

The experimental measurement testbed is shown in Fig. 3, which is composed of a VNA (Keysight E5061B, 5 Hz-3 GHz), a wide-band test fixture (Keysight 16197A, 3GHz) specifically designed for surface mounted components, a high-speed optical receiver (Newport Model-1601, 1GHz), a multi-mode optical fibre. All the measurements were carried out

at a room temperature of 20 °C. The LEDs mounted on the test fixture were driven using the reflection port of the vector network analyser with a 50 Ω output impedance, whereas the transmission port of VNA was used to monitor the output of the optical receiver. A short length multi-mode fibre was used to connect LED and the optical receiver. The VNA was calibrated prior to carrying out measurements. For each LED we carried out measurements for the impedance and S21 parameter for a range of bias voltage.

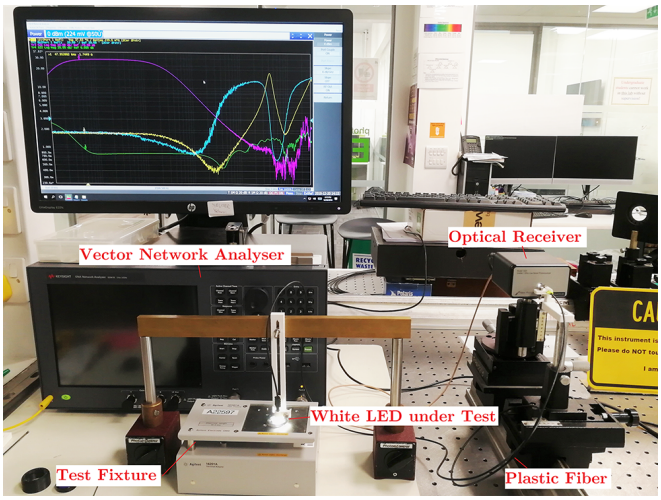


Fig. 3. Experimental setup

### A. V-I Measurement

Using a source meter (Keithley 2400), we measured the V-I curves for both LEDs as shown in Fig. 4. With the measured data, we carried out curve fitting using the *p-n* junction diode equation $I = I_S e^{q(V - IR_{S_{DC}})/nkT}$ with a parasitic series resistance $R_{s_{DC}}$, where $I_S$ is the reverse saturation current, $n$ is the ideal factor, $k$ is the Boltzman constant, $T$ is the absolute temperature, $q$ is the charge of an electron. Table I lists fitted parameters for two devices.

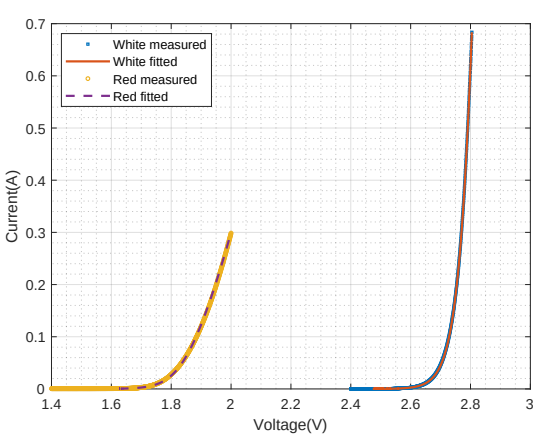


Fig. 4. Measured and fitted V-I curves of LEDs

TABLE I
PARAMETERS FITTED

| Description | White LED | Red LED |
|---|---|---|
| Reverse saturation current $I_S$ | $1.13 \times 10^{-35}$ A | $3.12 \times 10^{-21}$ A |
| Ideal factor $n$ | 1.34 | 1.98 |
| Series resistance $R_{s_{DC}}$ | 0.015 Ω | 0.360 Ω |

### B. Impedance Measurement

In order to ensure that LEDs are operating within the linear region, an AC signal with an output power of −40 dBm was used to measure the impedance for a range of bias voltage generated from the internal bias tee of the VNA's reflection port. The voltage across the LED was measured using a DC voltage meter in order to estimate the bias current with the help of V-I curves. Due to the high impedance of the voltage meter, the measured voltage can be used as an accurate estimate of voltage cross the LED. After measuring the DC voltage, the voltage meter was removed to eliminate its effect on the measurement results. The impedance results were captured from the VNA.

Figs. 5 and 6 show the measured impedance (only the magnitude vs the frequency is given here for clarity) of the white and red LEDs for a range of bias conditions. Tables II and III list the estimated values of the elements. To illustrate the fitting method and its accuracy, the impedance of the red LED biased at (1.7 V, 1.662 V, 4.0 mA), which represents the DC bias voltage of VNA, voltage across the LED and estimated current, respectively, is shown in Fig. 7. The LED behaves like a low pass filter in the low frequency range (see the inset at the left), and the first impedance floor can be estimated by $R_b + R_s + r_d$. With the frequency increasing, a second floor appears where $R_d$ is shorted by $C_j$ , thus making the corresponding value suitable to account for $R_b + R_s$ and the roll-off of the impedance to estimate $C_j$ . The lowest impedance dip is used to estimate $R_b$ at the resonance frequency of $(2\pi\sqrt{L_b C_b})^{-1}$ provided the following condition holds:

(1.7V, 1.662V, 4.0mA) is like (x,y,z) for bias voltages and current,see fig5,6. So I didn't add "and" here.

$$\left|\frac{1}{j\omega C_b}\right| \ll \left|R_s + \frac{1}{j\omega(C_{sc} + C_d)} // r_d\right| \tag{4}$$

At frequencies above the resonance peak, the impedance can be used to estimate $L_b$ since the parasitic inductance $L_b$ is dominant (see the inset at the right). However, if (4) is not met, then there will be inaccuracy in the estimation.

It has been observed that, the differential resistance estimated using $R_{S_{\mathrm{DC}}} + nkT/qI_0$ ($I_0$ is the bias current) accounts for $r_d$ in the model as well as $R_{\mathrm{sum}} = R_b + R_s + r_d$. This is evident from Tables II and III, and can be explained by the measured V-I curves, which can interpreted as the characteristics of the entire LED. Another observation is that, $R_s$ decreases as the bias current increases, which is different from those lasers and LEDs used in communication systems [15], [20].

TABLE II
PARAMETERS FITTED FOR THE WHITE LED

| Bias(V,mA) | $R_b(\Omega)$ | $C_b$(nF) | $L_b$(nH) | $R_s(\Omega)$ | $r_d(\Omega)$ | $C_j$(nF) | $R_{\text{sum}}(\Omega)$ | $nkT/qI_0 + R_{s_{DC}}(\Omega)$ |
|---|---|---|---|---|---|---|---|---|
| $(0.000, 0)$ | 0.20 | 3.36 | 2.45 | – | – | – | – | – |
| $(1.000, 0)$ | 0.20 | 3.65 | 2.45 | – | – | – | – | – |
| $(2.000, 0)$ | 0.20 | 4.19 | 2.45 | – | – | – | – | – |
| $(2.100, 0)$ | 0.20 | 4.45 | 2.45 | – | – | – | – | – |
| $(2.200, 0)$ | 0.20 | 4.99 | 2.45 | – | – | – | – | – |
| $(2.300, 0)$ | 0.20 | 6.17 | 2.45 | – | – | – | – | – |
| $(2.400, 0)$ | 0.20 | 8.16 | 2.45 | – | – | – | – | – |
| $(2.493, 0.2)$ | 0.20 | 10.5 | 2.45 | 55.52 | 206.28 | 0.1 | 261.2 | 286.5 |
| $(2.558, 0.8)$ | 0.20 | 12.2 | 2.45 | 15.24 | 30.13 | 0.1 | 45.57 | 44.47 |
| $(2.591, 2.1)$ | 0.25 | 13.7 | 2.45 | 2.84 | 14.35 | 0.2 | 17.45 | 17.28 |
| $(2.610, 3.5)$ | 0.27 | 14.4 | 2.45 | 2.61 | 7.07 | 0.2 | 9.95 | 10.03 |
| $(2.623, 5.0)$ | 0.27 | 14.4 | 2.45 | 2.67 | 3.94 | 4.0 | 6.88 | 6.91 |
| $(2.632, 6.5)$ | 0.28 | 14.4 | 2.45 | 2.42 | 2.51 | 7.9 | 5.21 | 5.34 |
| $(2.675, 22.7)$ | 0.28 | 14.4 | 2.45 | 0.58 | 0.72 | 15.8 | 1.58 | 1.57 |
| $(2.691, 35.8)$ | 0.28 | 17.0 | 2.45 | 0.42 | 0.33 | 28.9 | 1.02 | 1.00 |

TABLE III
PARAMETERS FITTED FOR THE RED LED

| Bias(V, mA) | $R_b(\Omega)$ | $C_b$(nF) | $L_b$(nH) | $R_s(\Omega)$ | $r_d(\Omega)$ | $C_j$(nF) | $R_{\text{sum}}(\Omega)$ | $nkT/qI_0 + R_{s_{DC}}(\Omega)$ |
|---|---|---|---|---|---|---|---|---|
| $(0.000, 0)$ | 1.78 | 0.29 | 0.99 | – | – | – | – | – |
| $(1.500, 0)$ | 1.60 | 0.23 | 0.99 | 7.60 | 4113.59 | 0.45 | 4122.79 | 1900.23 |
| $(1.595, 0.5)$ | 1.65 | 0.25 | 0.99 | 6.63 | 350.14 | 1.12 | 358.42 | 188.91 |
| $(1.662, 1.2)$ | 1.66 | 0.27 | 0.99 | 4.06 | 43.48 | 4.72 | 49.20 | 37.33 |
| $(1.694, 2.4)$ | 1.58 | 0.27 | 0.99 | 2.56 | 14.32 | 10.9 | 18.47 | 17.34 |
| $(1.715, 4.0)$ | 1.58 | 0.27 | 0.99 | 1.92 | 7.50 | 18.1 | 11.01 | 10.55 |
| $(1.730, 5.8)$ | 1.21 | 0.19 | 0.99 | 1.96 | 4.89 | 24.7 | 8.06 | 7.43 |
| $(1.770, 15.0)$ | 1.21 | 0.19 | 0.99 | 1.28 | 1.46 | 49.7 | 3.95 | 3.03 |
| $(1.794, 24.7)$ | 1.38 | 0.19 | 0.99 | 0.78 | 0.83 | 75.1 | 2.99 | 1.85 |
| $(1.813, 35.2)$ | 1.47 | 0.19 | 0.99 | 0.54 | 0.53 | 100 | 2.54 | 1.30 |
| $(1.829, 45.7)$ | 1.35 | 0.19 | 0.99 | 0.54 | 0.39 | 130 | 2.28 | 1.00 |

### *C. S21 Measurement*

For the S21 measurement, a higher AC input current was uesd to drive the LED in order to provide a sufficient optical power at the optical receiver. The AC power was increased accordingly for different bias conditions while keeping the measured impedance curves the same as what was measured with $-40$ dBm output power to ensure nonlinearity does not occur and the corresponding impedance models match.

Figs. 8 and 9 show the measured and estimated normalized S21 of the white and red LEDs. The estimated model shows a strong correlation with the red LED, however, the white LED response does not agree well with the model due to the effect of the phosphor coating [21] at low frequencies and inaccuracy of the impedance fitting at high frequencies. The second knee points followed by a $-60$ dB/dec slope caused by parasitic elements are predicted by the model and agree well with measured S21 parameter for the red LED. It has also been observed that the knee points for the white LED are highly correlated with the anti-resonance peaks.

## IV. CONCLUSION

The effective impedance measurement using the one-port reflection method was adopted to model the entire high power LED chip. The equivalent circuit model not only unveiled the impedance characteristics of those high power LEDs, but also provided an accurate way to estimate the frequency response in the optical domain. Extensive experiments were carried out to confirm the accuracy of this technique.

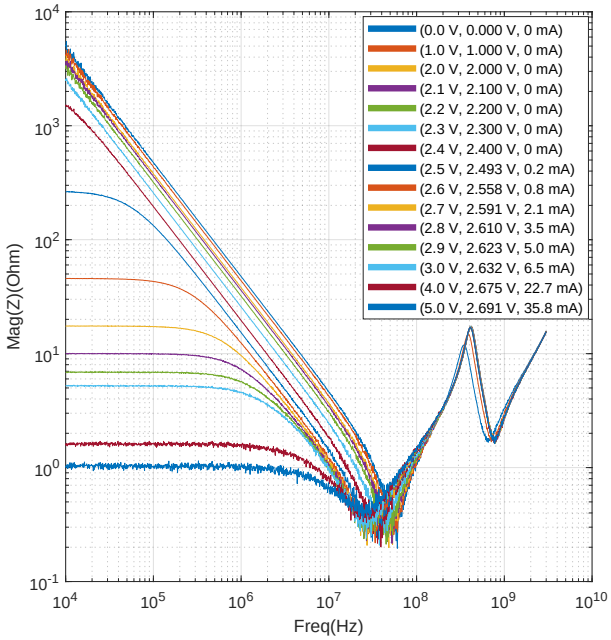


Fig. 5. Measured impedance of the white LED

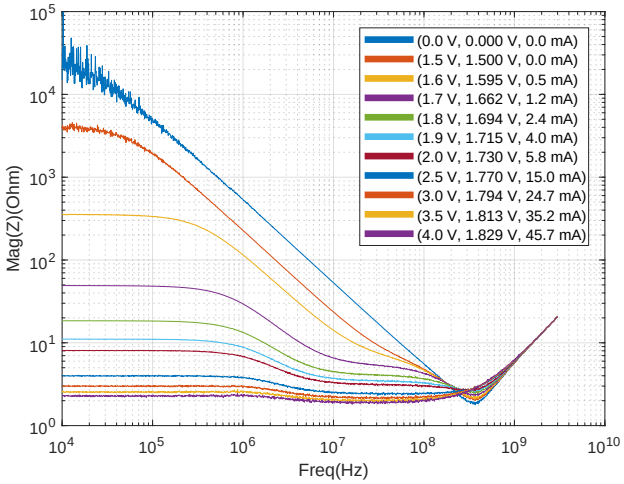


Fig. 6. Measured impedance of the red LED

## V. Acknowledgment

This work is supported by the European Unions Horizon 2020 research and innovation programme under the Marie Slodowska-Curie grant agreement n° 764461 (VISION), the UK EPSRC research grant EP/P006280/1: MARVEL and the Czech Science Foundation project GACR 17-17538S.

## References

[1] C. A. Burrus and R. W. Dawson, "Small-area high-current-density gaas electroluminescent diodes and a method of operation for improved degradation characteristics," *Applied Physics Letters*, vol. 17, no. 3, pp. 97–99, 1970.

[2] R. H. Saul, T. P. Lee, and C. A. Burrus, *Chapter 5 Light-Emitting-Diode Device Design*. Elsevier, 1985, vol. 22, pp. 193–237.

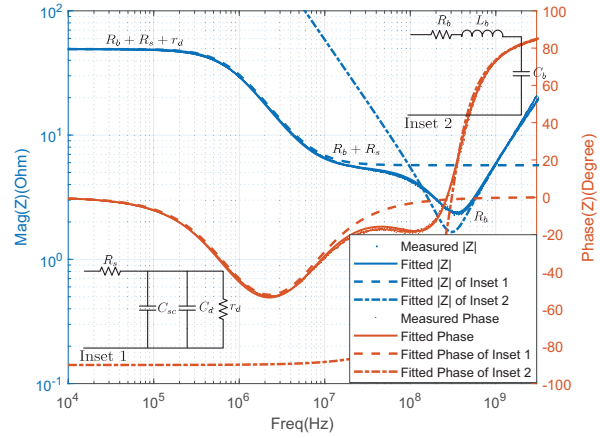


Fig. 7. Measured and fitted impedance of the red LED biased at 4.0 mA

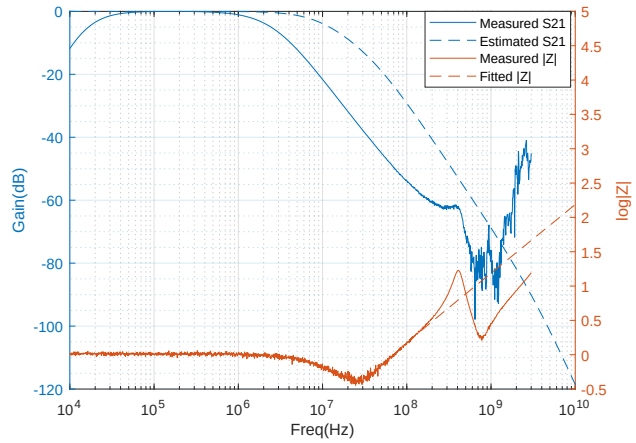


Fig. 8. Measured and fitted S21 of the white LED biased at 35.8 mA

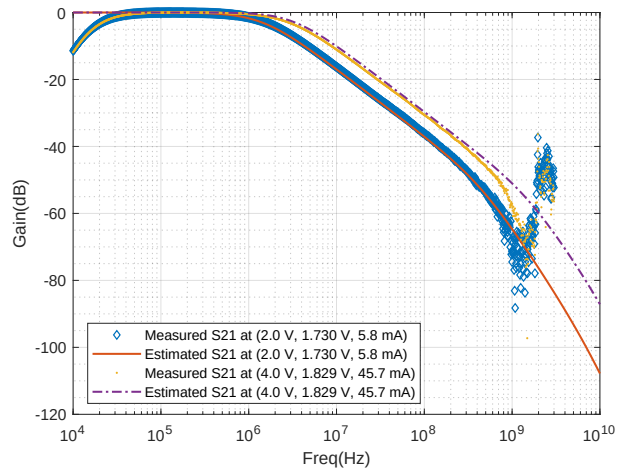


Fig. 9. Measured and fitted impedance of the red LED biased at 5.8 mA, 45.7 mA

[3] T. P. Lee, "Effect of junction capacitance on the rise time of led's and on the turn-on delay of injection lasers," *The Bell System Technical Journal*, vol. 54, no. 1, pp. 53–68, 1975.

[4] Y. S. Liu and D. A. Smith, "The frequency response of an amplitude-modulated gaas luminescence diode," *Proceedings of the IEEE*, vol. 63, no. 3, pp. 542–544, 1975.

[5] I. Hino and K. Iwamoto, "Led pulse response analysis considering the distributed cr constant in the peripheral junction," *IEEE Transactions on Electron Devices*, vol. 26, no. 8, pp. 1238–1242, 1979.

[6] G. P. Agrawal, *Fiber-optic communication systems*. John Wiley & Sons, 2012, vol. 222.

[7] M. Uysal, C. Capsoni, Z. Ghassemlooy, A. Boucouvalas, and E. Udvary, *Optical Wireless Communications: An Emerging Technology*. Springer, 2016.

[8] Z. Ghassemlooy, L. N. Alves, S. Zvanovec, and M.-A. Khalighi, *Visible Light Communications: Theory and Applications*. CRC Press, 2017.

[9] R. Tucker and I. Kaminow, "High-frequency characteristics of directly modulated InGaAsP ridge waveguide and buried heterostructure lasers," *Journal of Lightwave Technology*, vol. 2, no. 4, pp. 385–393, 1984.

[10] R. S. Tucker and D. J. Pope, "Microwave circuit models of semiconductor injection lasers," *IEEE Transactions on Microwave Theory and Techniques*, vol. 31, no. 3, pp. 289–294, 1983.

[11] R. Tucker and D. Pope, "Circuit modeling of the effect of diffusion on damping in a narrow-stripe semiconductor laser," *IEEE Journal of Quantum Electronics*, vol. 19, no. 7, pp. 1179–1183, 1983.

[12] R. S. Tucker, "Circuit model of double-heterojunction laser below threshold," *IEE Proceedings I - Solid-State and Electron Devices*, vol. 128, no. 3, pp. 101–106, 1981.

[13] M. Maeda, K. Nagano, M. Tanaka, and K. Chiba, "Buried-heterostructure laser packaging for wideband optical transmission systems," *IEEE Transactions on Communications*, vol. 26, no. 7, pp. 1076–1081, 1978.

[14] S. Maxim, C. Ashay, K. Alexey, Z. Jianping, A. Vinod, S. Grigory, and K. MuhammadAsif, "Differential carrier lifetime in algan based multiple quantum well deep uv light emitting diodes at 325 nm," *Japanese Journal of Applied Physics*, vol. 41, no. 10B, p. L1146, 2002.

[15] W. N. Cheung, P. J. Edwards, and G. N. French, "Determination of led equivalent circuits using network analyser measurements," in *Conference on Optoelectronic and Microelectronic Materials and Devices. Proceedings (Cat. No.98EX140)*, 1998, Conference Proceedings, pp. 232–235.

[16] S. Liu and X. Luo, *LED packaging for lighting applications: design, manufacturing, and testing*. John Wiley & Sons, 2011.

[17] J. H. Yu, W. Oepts, and H. Konijn, "Pc board thermal management of high power leds," in *Twenty-fourth Annual IEEE Semiconductor Thermal Measurement and Management Symposium*, 2008, Conference Proceedings, pp. 63–67.

[18] G. Chen, M. Craven, A. Kim, A. Munkholm, S. Watanabe, M. Camras, W. Gtz, and F. Steranka, "Performance of high-power iii-nitride light emitting diodes," *physica status solidi (a)*, vol. 205, no. 5, pp. 1086–1092, 2008.

[19] E. F. Schubert, *Light-emitting diodes*, 2018.

[20] A. Bacou, A. Hayat, V. Iakovlev, A. Syrbu, A. Rissons, J. Mollier, and E. Kapon, "Electrical modeling of long-wavelength vcsels for intrinsic parameters extraction," *IEEE Journal of Quantum Electronics*, vol. 46, no. 3, pp. 313–322, 2010.

[21] G. Stepniak, M. Schppert, and C. Bunge, "Advanced modulation formats in phosphorous led vlc links and the impact of blue filtering," *Journal of Lightwave Technology*, vol. 33, no. 21, pp. 4413–4423, 2015.